

Extending the Hybrid Surgical Guidance Concept With Freehand Fluorescence Tomography

Matthias N. van Oosterom^{ID}, Philippa Meershoek, Mick M. Welling, Francisco Pinto, Philipp Matthies, Hervé Simon, Thomas Wendler, Nassir Navab, Cornelis J. H. van de Velde, Henk G. van der Poel, and Fijis W. B. van Leeuwen^{ID}

Abstract— Within image-guided surgery, ‘hybrid’ guidance technologies have been used to integrate the complementary features of radioactive guidance and fluorescence guidance. Here, we explore how the generation of a novel freehand fluorescence (fhFluo) imaging approach complements freehand SPECT (fhSPECT) in a hybrid setup. Near-infrared optical tracking was used to register the position and the orientation of a hybrid opto-nuclear detection probe while recording its readings. Dedicated look-up table models were used for 3D reconstruction. In phantom and excised tissue settings (i.e., flat-surface human skin explants), fhSPECT and fhFluo were investigated for image resolution and in-tissue signal penetration. Finally, the combined potential of these freehand technologies was evaluated on prostate and lymph node specimens of prostate cancer patients receiving prostatectomy and sentinel lymph node dissection (tracers: indocyanine green (ICG) + ^{99m}Tc-nanocolloid or ICG-^{99m}Tc-nanocolloid). After hardware and software integration, the hybrid setup created 3D nuclear and fluorescence tomography scans. The imaging

Manuscript received April 12, 2019; revised June 14, 2019; accepted June 15, 2019. Date of publication June 21, 2019; date of current version December 27, 2019. This work was supported in part by the European Research Council under Grant 323105 and in part by the NWO-TTW-VICI Grant TTW 16141. (Corresponding author: Fijis W. B. van Leeuwen.)

M. N. van Oosterom is with the Interventional Molecular Imaging Laboratory, Department of Radiology, Leiden University Medical Center, 2333 ZA Leiden, The Netherlands, and also with the Department of Surgery, Leiden University Medical Center, 2333 ZA Leiden, The Netherlands (e-mail: m.n.van_oosterom@lumc.nl).

P. Meershoek and F. W. B. van Leeuwen are with the Interventional Molecular Imaging Laboratory, Department of Radiology, Leiden University Medical Center, 2333 ZA Leiden, The Netherlands, and also with the Department of Urology, Netherlands Cancer Institute–Antoni van Leeuwenhoek Hospital, 1066 CX Amsterdam, The Netherlands (e-mail: f.w.b.van_leeuwen@lumc.nl).

M. M. Welling is with the Interventional Molecular Imaging Laboratory, Leiden University Medical Center, 2333 ZA Leiden, The Netherlands.

F. Pinto and P. Matthies are with Health Data Pioneers GmbH, 81671 Munich, Germany.

H. Simon is with Eurorad SA, 67201 Eckbolsheim, France.

T. Wendler is with Computer Aided Medical Procedures, Technical University Munich, 85748 Munich, Germany, and also with SurgicEye GmbH, 81671 Munich, Germany.

N. Navab is with Computer Aided Medical Procedures, Johns Hopkins University, Baltimore, MD 21218 USA, and also with Computer Aided Medical Procedures, Technical University Munich, 85748 Munich, Germany.

C. J. H. van de Velde is with the Department of Surgery, Leiden University Medical Center, 2333 ZA Leiden, The Netherlands.

H. G. van der Poel is with the Department of Urology, Netherlands Cancer Institute–Antoni van Leeuwenhoek Hospital, 1066 CX Amsterdam, The Netherlands.

Color versions of one or more of the figures in this article are available online at <http://ieeexplore.ieee.org>.

Digital Object Identifier 10.1109/TMI.2019.2924254

resolution of fhFluo (1 mm) was superior to that of fhSPECT (6 mm). Fluorescence modalities were confined to a maximum depth of 0.5 cm, while nuclear modalities were usable at all evaluated depths (<2 cm). Both fhSPECT and fhFluo enabled augmented- and virtual-reality navigation toward segmented image hotspots, including relative hotspot quantification with an accuracy of 3.9% and 4.1%. Imaging in surgical specimens confirmed these trends (fhSPECT: in-depth detectability, low resolution, and fhFluo: superior resolution, superficial detectability). Overall, when radioactive and fluorescent tracer signatures are used, fhFluo has complementary value to fhSPECT. Combined the freehand technologies render a unique hybrid imaging and navigation modality.

Index Terms— Image-guided surgery, augmented reality, fluorescence tomography, surgical navigation, freehand SPECT, hybrid imaging.

I. INTRODUCTION

INTRAOPERATIVE tissue identification is often of paramount importance to achieve an effective and minimal invasive surgical procedure. One of the most frequently used surgical guidance methods encompasses the use of radioactive tracers that specifically accumulate in targeted tissues (e.g. tumorous tissue [1]), facilitating complete resection of the targeted tissue (e.g. clear tumor boundaries [2], [3]) and sparing of healthy tissue (e.g. lymphatics [4]). Since the high penetration depth of gamma rays allow for sensitive detection of the tracer-targeted tissues deep within the patient anatomy, radioguided surgery can be considered the ‘gold standard’ for interventional molecular imaging [5]. These nuclear medicine qualities enable surgical planning via 3D preoperative imaging (e.g. single-photon emission computed tomography/X-ray computed tomography (SPECT/CT)) and intraoperative in-depth guidance via handheld gamma ray detection probes or mobile gamma cameras [6]. The latter can even be extended to 3D intraoperative tomographic imaging via freehand SPECT (fhSPECT) imaging [7], [8]. Surgical guidance has a large visual component, a feature that is lacking in traditional radioguidance procedures.

Fluorescence guidance has emerged as an optical alternative for surgical guidance and is rapidly being adopted in many different interventional settings [9]. Unfortunately, fluorescence guidance can only be used for superficially located lesions, since light suffers from severe attenuation, scatter and reflection in tissue. This restricts fluorescent penetration to a maximum of roughly 1 cm deep in tissue [10].

This limits in-depth visibility, but prevents shine-through of underlying tracer distributions and as such facilitates the identification of superficial lesions located in close proximity to high background signals [11], [12]. Moreover, when used superficially, fluorescence imaging can be performed with a superior spatial resolution when compared to gamma ray detection [11], even enabling (real-time) microscopic investigation [13], [14]. Although 3D fluorescence imaging in the form of a fluorescence tomography setting has been reported for pre-interventional breast cancer diagnosis [15], to our knowledge, 3D or pseudo 3D fluorescence imaging has not yet been attempted in an image-guided surgery setting.

To further improve the accuracy of image-guided surgery, it seems logical to make use of hybrid strategies that combine radioactive and fluorescent signatures [16], thereby creating a best-of-both-worlds scenario. Multiplexing of the complementary signatures allows for surgical guidance concepts that harbor the advantages of the individual technologies, e.g. 3D preoperative radionuclide imaging and intraoperative optical guidance [16], [17]. Acquiring both radioactive and fluorescent signals for (intraoperative) tissue identification can be achieved by applying two separate tracers, but more ideally is achieved using a single tracer that contains both the complementary emission types, yielding a so-called ‘dual-modality’ or ‘hybrid’ tracer. Extensive use of free indocyanine green (ICG) in combination with ^{99m}Tc -nanocolloid [10], [18]–[20] or the hybrid tracer ICG- ^{99m}Tc -nanocolloid in clinical sentinel lymph node (SN) biopsy trials [11], [12], [21]–[23], has underlined the value of the hybrid surgical guidance concept.

This successful clinical exploration of the hybrid surgical guidance concept has provided the basis for the development and clinical evaluation of a range of intraoperative hybrid detection modalities [24], [25]. The first reported clinically applied hybrid modality, which is now also commercially available, is the so-called opto-nuclear probe (Eurorad S.A., Eckbolsheim, France) [26]–[28]. In this device, numeric and acoustic gamma tracing is combined with numeric and acoustic tracing of the fluorescent dye ICG with a one channel optical detector. To our knowledge, fully integrated image-based hybrid gamma and fluorescence cameras have only been reported in the preclinical setting so far [29]–[31]. However, to study the potential of such an image-based hybrid modality during surgery, clinical studies have been performed in a setting wherein a tailored bracket was used to physically connect a gamma probe or a portable gamma camera to a fluorescence exoscope [32]. Key advantages of the hybrid modalities appeared to be: 1) the ability to use in-depth radioguidance to guide positioning of fluorescence imaging; 2) logistical simplification in the operating room.

Alternative to hybrid imaging devices, hybrid surgical navigation concepts have been used to successfully integrate the nuclear guidance as provided by preoperative SPECT or intraoperative fhSPECT images with fluorescence guidance [33]–[36]. Key advantages of the hybrid navigation approach appeared to be: 1) the ability to provide augmented reality displays of radioactive findings in a fluorescence video display; 2) virtual- or augmented-reality “video-game like” guidance of the fluorescence camera to the lesions

(with numerical feedback of the distance to the lesion). While a complete hardware integration can also provide value when separate tracers are used for the radioactive and fluorescent signatures, e.g. separating targeted tissue from healthy tissue [37], success of this navigated fluorescence camera approach relies on a direct link between SPECT and fluorescence findings, thus requiring a single hybrid tracer.

Based on the assumption that radioactive and fluorescence guidance provide complementary information during surgery, we have now studied the integrated use of ICG- ^{99m}Tc -nanocolloid, the opto-nuclear hybrid detection modality and a modified fhSPECT navigation platform (see Fig. 1). To allow for hybrid imaging and navigation, fhSPECT was complemented by a new form of (pseudo-) 3D intraoperative fluorescence tomography that we call freehand fluorescence (fhFluo). To investigate if and how fhFluo imaging adds complementary information during surgical guidance, both fhSPECT and fhFluo technologies were evaluated in a phantom setup and initial clinical validation was performed on surgical specimens.

II. METHODS AND MATERIALS

A. Integration of the Opto-Nuclear Probe With the DeclipseSPECT Navigation Device

The hybrid fhSPECT and fhFluo setup depicted in Figure 1 was realized using the declipseSPECT navigation device (SurgicEye GmbH, Munich, Germany) [7], [8] and the opto-nuclear probe [27], capable of both gamma and fluorescence measurements in counts/s. As described by Van den Berg *et al.*, the fluorescence measurements are acquired with two acrylic optical fibers, each containing a numerical aperture of 0.51 and a diameter of 1 mm. The first fiber is coupled to a 785 nm laser for excitation of the fluorescence dye ICG, providing a typical optical power of 3.7 mW/cm^2 at the fiber output. The second fiber is coupled to a $> 810 \text{ nm}$ optical filter and an infrared-extended photomultiplier tube (H10721-20, Hamamatsu Photonics kk., Hamamatsu, Japan) to collect the fluorescence emission signals. The resulting system sensitivity for ICG, in terms of minimum detectable ICG concentration, was previously reported as $< 0.061 \text{ ng/mL}$ [27]. To enable position- and orientation-tracking of the opto-nuclear probe, the navigation system applies near-infrared (NIR) optical tracking (Polaris Vicra, Northern Digital Inc., Waterloo, Canada) of a four-fiducial reference target, specifically designed to attach at the distal end of the probe (see Fig. 1b). To geometrically calibrate the position of the gamma- or fluorescence-entrance windows with respect to this reference target, thereby tracking both gamma and fluorescence detection locations, individual geometrical calibrators were designed using SolidWorks computer-aided design software (Dassault Systèmes SA, Vélizy-Villacoublay, France), similar as previously described by Van Oosterom *et al.* [35]. These were 3D printed (acrylonitrile butadiene styrene plastics; Dimension Elite 3D printer, Stratasys Ltd., Eden Prairie, MN, USA) and used to calibrate the position of the respective detectors relative to the fiducials at the distal end of the opto-nuclear probe [35]. An oscilloscope (PicoScope,

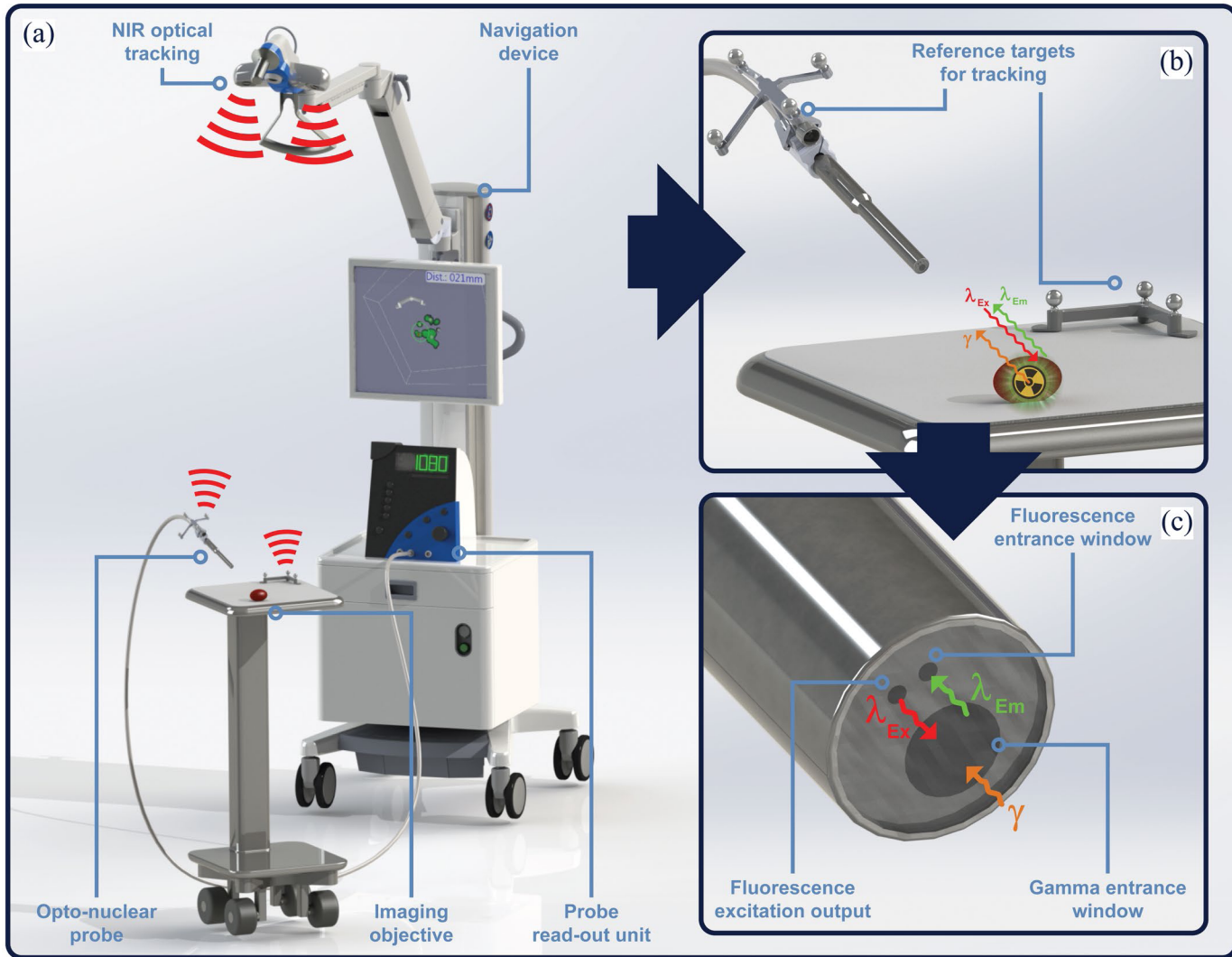


Fig. 1. Schematic overview of the hybrid imaging and navigation modality. (a) Overview of the total setup, showing near-infrared (NIR) tracking of both the opto-nuclear probe and the imaging objective. (b) Zoom-in of the opto-nuclear probe and imaging objective, displaying the presence of both a radioactive (γ) and fluorescent ($\lambda_{\text{Excitation}}$ and $\lambda_{\text{Emission}}$) tracer signature in the imaging objective. (c) Zoom-in of the probe entrance windows for nuclear and fluorescence detection.

Pico Technology Ltd., Cambridgeshire, UK) housed within the declipseSPECT was used to transfer the probe-read-out signals to the declipseSPECT, either via an analogue signal (nuclear read-out of the gamma signal) or a digital transistor-transistor-logic signal (optical read-out of the fluorescence signal).

By simultaneously recording the position and orientation of the opto-nuclear probe and its 1D probe readings (sample rate of 0.5 s), software algorithms could be used to extrapolate the geometrical source location of the readings. A modified version of the declipse 6.0 software (SurgicEye GmbH) was used to reconstruct a tomographic 3D volume based on the gamma readings (i.e. an fhSPECT scan as previously described [8], [38]–[40]). A tomographic 3D reconstruction of the fluorescence readings (i.e. a fhFluo scan) was realized in analogy to the well validated fhSPECT technology. The underlying mathematical models used were based on previously validated look-up table (LUT) methods [38], [39], [41];

The LUT model provides an estimate of which voxels in the scanning volume could have contributed, and with what kind of weight, to the individual probe measurements. In line with previous reports, a maximum likelihood expectation maximization algorithm was used to approximate the actual tracer distribution within the volume [39], [42]. For the fhSPECT part, the reconstruction model was configured, as previously described, by using a dedicated LUT model based on nuclear Monte-Carlo simulations [39]. For fhFluo imaging, however, the real-measurements fluorescence LUT model was implemented [39]. This fluorescence LUT was obtained by measuring the response of a point source (6 $\mu\text{g/mL}$ ICG dissolved in epoxy resin with a total volume of about 1.5 μL [43]) in air using a sample volume of 11x11x10 mm and a resolution of 1 mm. Subsequently, the acquired LUT model was filtered with a Gaussian filter (size: 1 mm standard deviation) in order to compensate for measurement and calibration inaccuracies, and subsequently normalized.

TABLE I
MOST IMPORTANT DIFFERENCES IN FREEHAND SPECT AND
FLUORESCENCE RECONSTRUCTION AND
NAVIGATION SETTINGS

Reconstruction parameter	fhSPECT	fhFluo
Number of voxels	392000	392000
Voxel size (mm)	2x2x2	1x1x1
VOI size (voxels)	70x70x80	140x140x20
VOI size (mm)	140x140x160	140x140x20
Filter size (standard deviation, mm)	2	1
Acquisition + reconstruction time (typical range in min)	1-3	1-3
Navigation parameter	fhSPECT	fhFluo
Minimal scan hotspot size (mm)	1.2	0.6
Scan colormap	Green-blue-purple	Green-white
Augmented navigation target size (mm)	4	4
Augmented navigation target color	Red (when targeted) Gray (when not targeted)	Red (when targeted) Gray (when not targeted)

During both fhSPECT and fhFluo scan acquisition, the opto-nuclear probe was manually moved over and around the subject (no-tissue contact), thereby measuring at as many different positions and orientations as possible within a < 5 min acquisition time [8]; Previous clinical experience with fhSPECT during surgery suggests total scanning time should be kept roughly below 5 min [8], [44], [45] (see Table 1).

To geometrically link the position and orientation of the resulting scan to the imaged objective, thereby allowing for augmented reality overlay or subsequent navigation, a three-fiducial reference target, also tracked by the aforementioned tracking system, was attached nearby the specimen under study (see Fig. 1b). When the fhSPECT and fhFluo scans were deployed for 3D surgical navigation, the intensity hotspots in the reconstructed tracer distribution functioned as the navigation targets (e.g. SN locations within the specimen). These navigation targets were segmented automatically, which occurred based on the weighted center of gravity of the intensity hotspots. Subsequent augmented and/or virtual reality visualizations where shown from the perspective as approached by the navigation instruments using the modified declipse 6.0 software.

B. Patients

Ex vivo human skin explants were obtained from an abdominal skin reduction procedure. SN and prostate samples were acquired from five prostate cancer patients receiving a combination of robot-assisted laparoscopic SN biopsy, extended pelvic lymph node dissection (ePLND) and prostatectomy. The prostate and dissected SN's contained either the hybrid tracer ICG-^{99m}Tc-nanocolloid or a combination of 'free' ICG and ^{99m}Tc-nanocolloid [19]. All procedures performed were in accordance with the ethical approval of our institutions

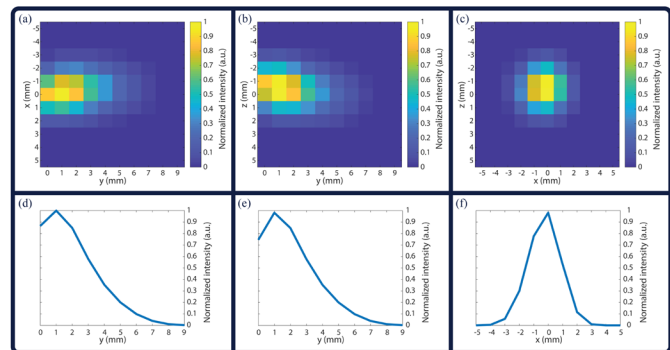


Fig. 2. Overview of the ICG fluorescence look-up table. (a-c) Maximum intensity projections of the look-up table, shown from three different directions, where the y-axis depicts the longitudinal axis of the opto-nuclear probe. (d-f) Horizontal line profiles taken at the middle of the maximum intensity projections as shown above.

(B18-009, NL46580.031.13 and NL57838.031.16) and the Helsinki Declaration.

C. Reference Modalities

As reference to the hybrid 3D fhSPECT and 3D fhFluo imaging setup, all measurements were also performed with more traditional image-guided surgery modalities [24], [25]. This included a handheld gamma camera (CrystalCam with low energy high resolution collimator and 30 s exposure time; Crystal Photonics GmbH, Berlin, Germany) and an open surgery fluorescence camera (FIS-00, Hamamatsu Photonics kk., Hamamatsu, Japan). This fluorescence camera is based on the previously reported m-PDE prototype system, harboring a CCD camera with > 820 nm optical longpass filter and a ring of LEDs for ICG excitation (755 nm center wavelength; 10 nm full-width-at-half-maximum) [43], [46]. In terms of minimum detectable ICG concentration, the sensitivity is reported as < 0.0093 ng/mL [46].

D. Image Resolvability and Quantification

To demonstrate the differences in imaging resolvability and resolution characteristics, a resolvability phantom was created. This phantom consisted of a 10 mm thick polymethylmethacrylate transparent plastic plate, where 12 well pairs were drilled with decreasing distances between the edges, ranging from 18 to 0.25 mm edge-to-edge. Each well was filled with a 170 μ L solution of the hybrid tracer ICG-^{99m}Tc-nanocolloid containing 1.03×10^{-2} mg/mL ICG and 2 MBq ^{99m}Tc. These values are in the range of a typical SN size and tracer concentration as reported for prostate cancer [47]. All well pairs were repeatedly scanned with the fhSPECT, fhFluo, CrystalCam and FIS-00 imaging modalities. The whole experiment was performed in duplicate, resulting in 48 different wells, imaged within 12 scans per imaging modality (i.e. 4 wells per image). To determine the significance in differences between relative image-hotspot quantification, an unpaired samples t-test with confidence interval of 95% was used in IBM SPSS statistics 22 software (International Business Machines Corp., New York, USA).

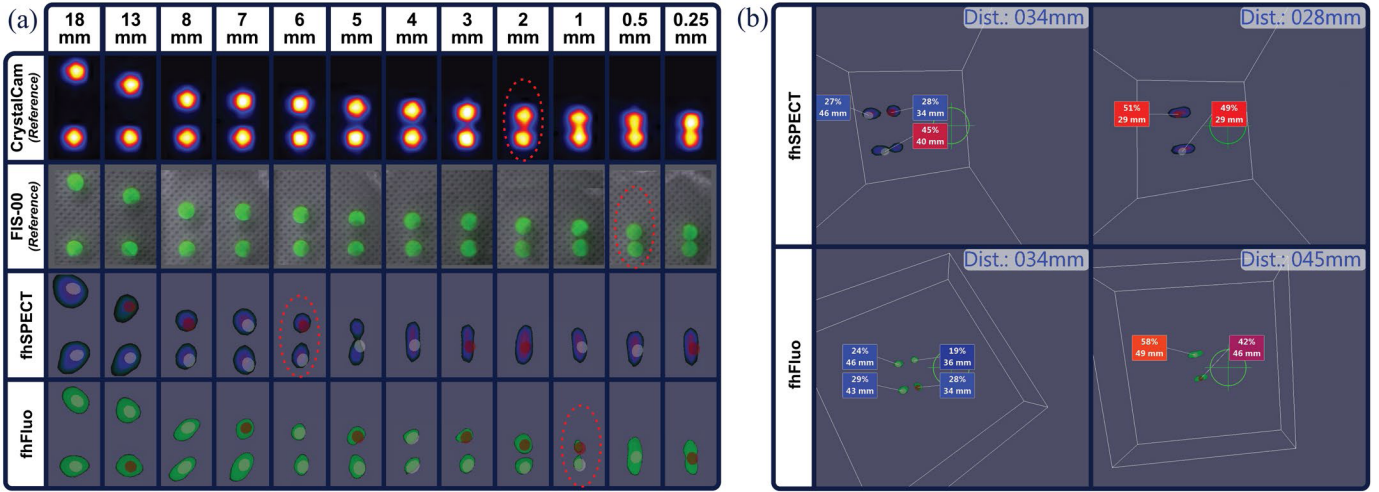


Fig. 3. Freehand SPECT and freehand Fluorescence imaging resolvability, navigation and relative hotspot quantification. **(a)** Results for image resolvability, based on two tracer sources located at varying distances with respect to each other, including the CrystalCam and FIS-00 reference modalities. A red dotted oval indicates the resolvability limit. **(b)** Example images of the virtual navigation and relative tracer quantification found for the segmented hotspots. The distance displayed is the distance estimated between the opto-nuclear probe tip and center of the navigation target aimed at.

E. Signal Penetration in Tissue

The influence of tissue attenuation was determined using human skin tissue (roughly a flat surface of 20 x 15 cm with a depth of 5 cm). To allow these investigations, an Eppendorf tube (Eppendorf AG, Hamburg, Germany) was filled with ICG-^{99m}Tc-nanocolloid (according to the above-mentioned volume and concentration), positioned at different depths from the skin surface (0, 0.5, 1 and 1.5 cm) and analyzed with the available imaging modalities.

F. Surgical Specimen Evaluation

In the operating room, excised specimens of the SNs and the prostate (i.e. the injection site of the tracer) were subjected to imaging with the fhSPECT, fhFluo, CrystalCam and FIS-00 modalities.

III. RESULTS

A. Integration of the Opto-Nuclear Probe With the DeclipseSPECT Navigation Device

Figure 2 shows a maximum intensity projection of the filtered fluorescence LUT model from different sides. The y-axis is depicted as the longitudinal axis of the probe. Interestingly, most likely due to the two-fiber setup (i.e. emitting and receiving), the acquired LUT model was not symmetrical and the maximum response was slightly in front of the probe ($y = 1$ mm). A curve along the longitudinal axis of the probe revealed a quick detection fall-off (100% at 1 mm, 50% at 3.3 mm, 10% at 6 mm and 5% at 6.8 mm). These findings are contrary to a typical LUT for gamma ray detection (^{99m}Tc) [39], which is symmetrical, has maximal response at the edge of the probe ($y = 0$ mm) and displays a more extended detection fall-off (100% at 0 mm, 50% at 5 mm, 10% at 19 mm and 5% at 33 mm).

Due to the above-mentioned detection differences, the customized fhFluo software was configured different to that of the fhSPECT (settings are shown in table 1). To accommodate

for the quick detection fall-off and typical tissue attenuation of fluorescent signals [9], [48], the volume of interest (VOI) used for the fhFluo scans was limited to a depth of 20 mm, while the fhSPECT VOI depth was configured at 160 mm. For both fhSPECT and fhFluo imaging options, scan reconstruction was performed ‘on-the-fly’ (i.e. during the 1-3 min scan acquisition). To ensure similar software performance, the number of voxels (392000) used was equal for both modalities. As a result, the reduced scan volume of the fhFluo yielded two-fold smaller voxel dimensions as compared to the fhSPECT scans.

B. Imaging Resolvability and Quantification

Figure 3a depicts the distinct differences in the resolvability outcomes obtained using the different modalities. The FIS-00 displayed the highest resolution: allowing separation at an edge-to-edge distance of 0.5 mm. The newly introduced fhFluo was second best, discriminating sources at 1 mm edge-to-edge. The CrystalCam came third with a resolvability of 2 mm, while the fhSPECT came last with a resolvability of 6 mm.

For the freehand imaging options the declipse 6.0 software was able to segment separate navigation targets for the tracer sources (depicted as virtual red and gray targets within the image hotspots; see Fig. 3). Because of this segmentation, navigation and relative hotspot quantification became possible (see Fig. 3b). For the latter, analysis of the fhSPECT images of the resolvability phantom yielded an average absolute inaccuracy of $3.9 \pm 3.3\%$. The average absolute inaccuracy for the hotspot quantification found in fhFluo was $4.1 \pm 2.7\%$. A paired-samples t-test revealed no significant difference between the quantification inaccuracies of both imaging modalities (p -value of 0.371).

C. Signal Penetration in Tissue

To study how the different modalities cope with the differences in tissue attenuation between radioactive and fluorescent signatures, in-depth detectability (≤ 2 cm) was

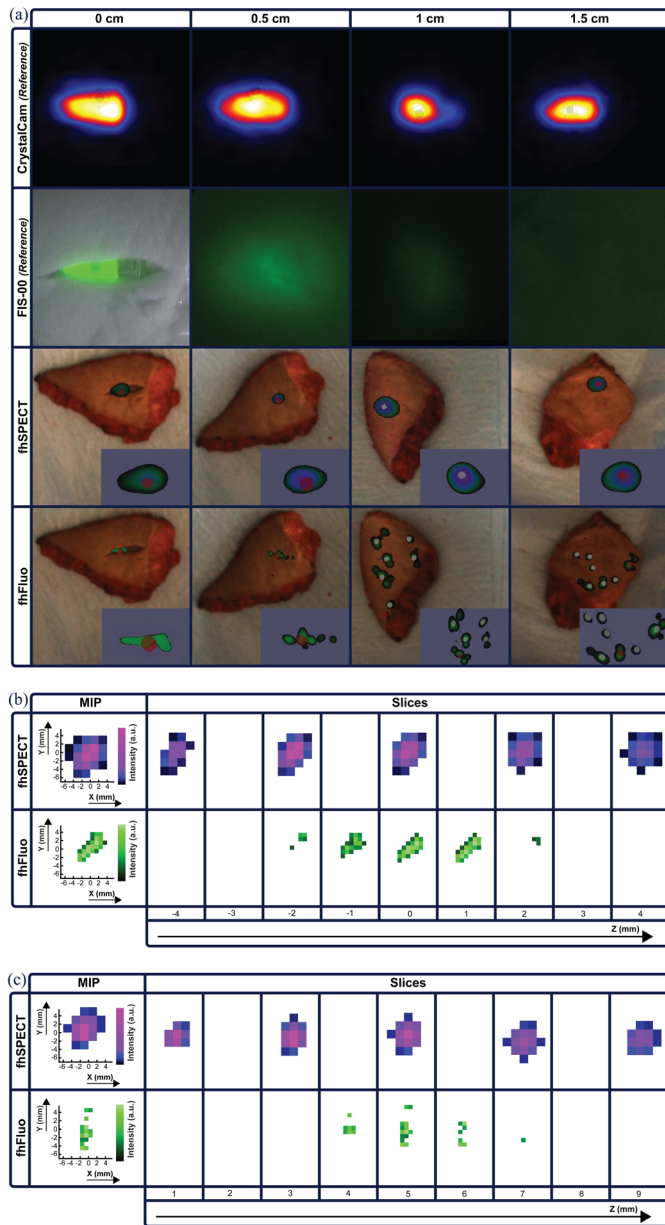


Fig. 4. Signal penetration in tissue for freehand SPECT and freehand fluorescence imaging, including CrystalCam and FIS-00 reference modalities. (a) Overview of all modalities. With a tracer source located at different depths in human skin, nuclear imaging (CrystalCam and fhSPECT) was useable at all depths, fluorescence imaging (FIS-00 and fhFluo) only up to 0.5 cm. However, source delineation (i.e. image resolution) was highest with fluorescence imaging at these superficial depths. (b) Zoomed-in look at the raw tomographic slices (using Matlab, MathWorks Inc.) of the freehand SPECT and freehand fluorescence 3D reconstructions with the tracer source at a depth of 0 cm, where MIP stands for maximum intensity projection. (c) Similar tomographic slices at 0.5 cm depth.

studied in human skin (see Fig. 4). Again, the imaging modalities revealed distinct differences. The sources could be detected at all evaluated depths using the two nuclear imaging options (i.e. handheld gamma camera and fhSPECT). However, the shapes best seem to match that of the actual source at a 0 cm depth. In line with the resolvability experiments, the shape of the source was displayed with more detail

(i.e. a higher resolution) using the fluorescence modalities. This advantage, however, disappeared at a > 0.5 cm depth due to clear signs of signal attenuation and diffusion. The FIS-00 camera did show a very diffuse fluorescence signal at 1 cm depth, though one could question if such a signal would provide valuable guidance during surgery. The observed attenuation and diffusion trends are in line with previous studies reporting the head-to-head comparison of signal penetrations in a phantom model [48].

D. Surgical Specimen Evaluation

Studies in surgical specimens containing ICG-^{99m}Tc-nanocolloid (see Figures 5 and 6), demonstrated that the fluorescence imaging modalities (i.e. FIS-00 and fhFluo) created a more detailed image of the (superficial) tracer distribution than the nuclear imaging options (i.e. CrystalCam and fhSPECT). Especially in the larger tissues, multiple small foci became visible with fluorescence modalities, while the nuclear modalities only showed a low number of large hotspots. When ICG and ^{99m}Tc-nanocolloid were administered separately, a clear difference in signal distribution was observed in the SN and prostate specimens (see Fig. 5). This is in line with the reported differences in tracer distribution kinetics [49].

Both fhSPECT and fhFluo allowed for navigation towards the middle of the segmented hotspots in augmented- and virtual-reality views (see Fig. 6). During navigation the numerical distance to the tip of the navigated opto-nuclear probe was displayed in real-time. When used for navigation on the larger prostate samples, fhSPECT allowed for in-depth navigation towards the large hotspot(s) (“tomographic imaging”), while fhFluo allowed for navigation towards multiple superficial hotspots (“pseudo-tomographic imaging”). Combined the two technologies provided superior superficial and in-depth tomographic imaging.

IV. DISCUSSION

In this study we have evaluated the integrated use of fhSPECT and fhFluo with a hybrid navigation concept for application in image-guided surgery. In such a setting, the complementary advantages of both nuclear and fluorescence imaging could be harnessed in a single setup. Hybrid freehand imaging offered a couple of additional features, not provided by more traditional hybrid systems: 1) 3D insight in to the tracer distribution (see Figures 3b, 4 and 6); 2) AR overlay of the reconstructed scan, including guidance features (see Figures 4, 5 and 6); 3) navigation towards the imaged lesions (see Figures 3b and 6); and 4) hotspot quantification within the image (see Fig. 3b). Current fhSPECT and fhFluo acquisition times ($\sim 1\text{-}5$ min) are long when compared to 2D handheld gamma cameras ($\sim 5\text{-}60$ sec) or 2D fluorescence cameras (real time). However, by increasing both computing power and device sensitivity, future technical refinements (e.g. higher sample rates) are likely to reduce these scan times. Furthermore, tissue deformation in between the freehand scan acquisition and actual surgical targeting can influence the actual navigation accuracy [50]. The true extend of these limitations, however, only becomes apparent during clinical

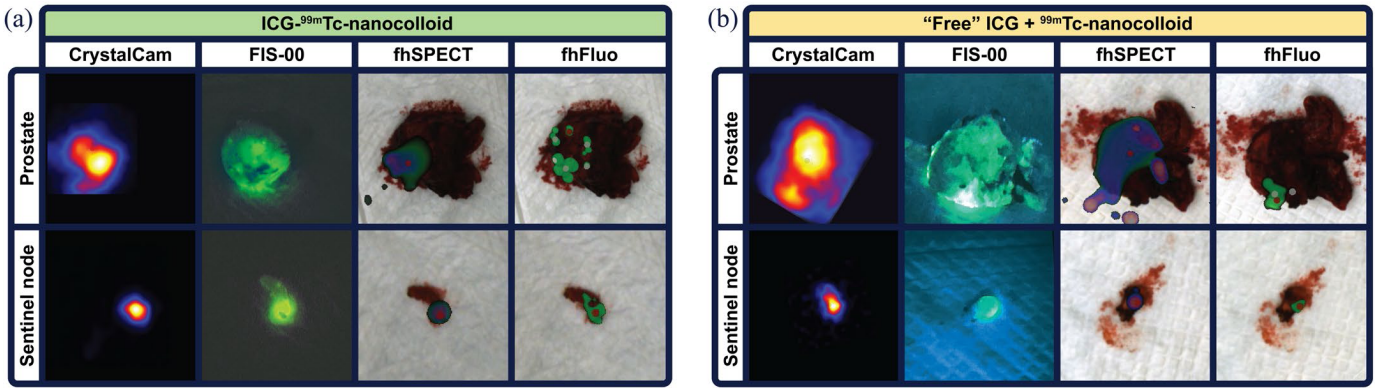


Fig. 5. Imaging of prostate and sentinel lymph node specimens using freehand SPECT and freehand fluorescence, including CrystalCam and FIS-00 reference modalities. (a) Examples of imaging when a single hybrid tracer ($\text{ICG-}^{99\text{m}}\text{Tc-nanocolloid}$) is used. (b) Examples of imaging when two separate tracers are used (“free” $\text{ICG} + {^{99\text{m}}\text{Tc-nanocolloid}}$). A small difference in color is visible between the FIS-00 images due to a difference in recording facilities available.

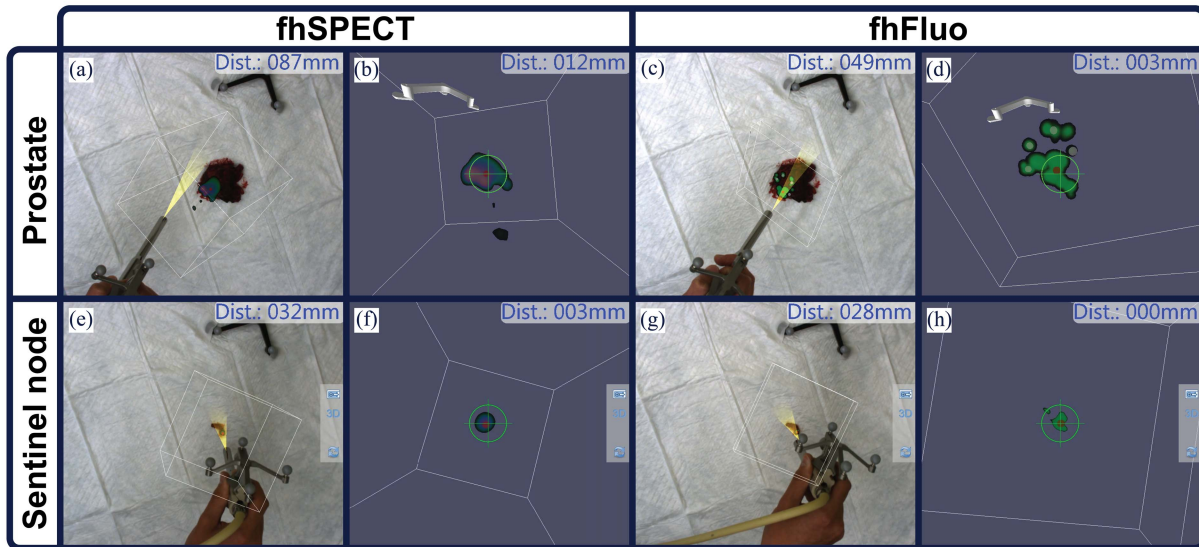


Fig. 6. Navigation on prostate and sentinel lymph node samples, based on freehand SPECT and freehand fluorescence imaging. (a, c, e and g) Examples of navigation in an augmented reality view. (b, d, f and h) Examples of navigation in a virtual reality view, where the tip of the opto-nuclear probe is positioned against the tissue surface. All distances shown are the estimated distances between the probe tip and the center of the navigated target.

implementation of the technology. Luckily, the real-time audible and numerical feedback delivered by the opto-nuclear probe [27] will help make sure the procedural accuracy is not at risk [51].

Phantom measurements indicated that the surface resolution of the prototype fhFluo option was superior to that of fhSPECT (see Fig. 3a) and hotspot quantification showed an equal accuracy (see Fig. 3b). NIR optical tracking can obstruct NIR fluorescence imaging setups [34], [43]. Interestingly, obstruction of the opto-nuclear probe detection only occurred when the detector was positioned within an unrealistic 15 cm from the optical tracking light source; the opto-nuclear probe is typically used at a working distance of 100-250 cm with respect to the tracking device. Further optimization of the underlying physical detection models is likely to refine future fhFluo reconstructions. For example,

recently introduced Monte Carlo based software for simulating fluorescence imaging setups [52], [53] opens the door for high resolution ICG LUTs that even simulate tissue interaction effects. To prevent tissue deformations the opto-nuclear probe is not used in direct tissue contact. Consequently, the simulated LUTs will have to rely on a dynamic ratio of air and skin contributions, rendering this approach a challenging and computationally demanding task.

Despite the reduced resolution of fhSPECT, this freehand technology supports navigation towards deeper lying tracer deposits, a feature that could accommodate radical surgical excision through the use of safety margins (commonly $\sim 0.5\text{-}2 \text{ cm}$ [54]–[57]). In agreement with previous reports on freehand beta⁺ probe imaging (fhBeta⁺) [58], fhFluo underlines the limitations of using imaging signatures that suffer from severe tissue attenuation to establish in-depth

safety margins. On the bright side, the superficial nature of fhBeta⁺⁻ and fhFluo does provide a means to study surgical resection planes in detail with limited ‘shine-through’ effect from background signals [2], [41]. In such applications, the superior resolution of fhFluo provides valuable detail. As such, fhFluo imaging might provide a valuable method for *in vivo* 3D mapping of surgical resection margins, preventing positive margins and disease recurrence. By facilitating *in vivo* application during surgery, possibly in a navigation workflow, resection details could be provided before excision of the tumor mass. When fhFluo is adapted for other wavelengths, it may help provide an optical alternative for such indications where superficial tissue detection is in demand; e.g. glioblastoma surgery using 5-aminolevulinic acid fluorescence [59], or nerve sparing during prostatectomy using fluorescein and Cy5 [60]. Even after surgery, such fhFluo scans might also provide useful insight and confirmation, allowing for macroscopic tomographic depictions of the tracer distribution in targeted structures (e.g. tumor location and margins or nerve density), thereby extending what is possible using 3D pathology [61].

Globally, radioguidance is routinely applied during SN procedures, radioguided occult lesion localization and radioguided seed localization [6]. With the increasing use of the hybrid tracer ICG-^{99m}Tc-nanocolloid during SN procedures, the proposed hybrid image-guided surgery approach should be directly implementable in a broad range of indications: prostate cancer [62], penile cancer [63], breast cancer [22], various head and neck cancers [11], [23] and cervical cancer [21]. While the currently proposed fhFluo system is only applicable during open surgery procedures, the recently introduced laparoscopic opto-nuclear probe [28] indicates a translation towards laparoscopic procedures as well, similar as laparoscopic freehand SPECT [36], [64], [65]. In addition, radioguided surgery is also increasingly finding its way into receptor targeted tumor resections, such as the targeting of somatostatin [66] and prostate specific membrane antigen [1] positive tumors. Continuous preclinical developments in to tumor-receptor targeted hybrid tracers [67], [68] indicates that future use of the introduced technology can be envisioned when using e.g. PSMA I&F in prostate cancer [69], Cy5-¹¹¹In-DTPA-Tyr3-octreotate for neuroendocrine tumors [70], [¹¹¹In]-DTPA-trastuzumab-IRDye800 in breast cancer [71] or ¹¹¹In-girentuximab-IRDye800CW in renal cancer [17]. As shown in the current study, next to complementing fhSPECT imaging of hybrid tracers, fhFluo can also be used to independently visualize fluorescence tracers such as ICG. Multiplexing to discriminate between two tracers may be used to e.g. intraoperatively differentiate between healthy and diseased lymphatic structures [37].

Analogous as to how we use our smartphones with global positioning system (GPS) navigation to direct ourselves through a map of the city in every-day life, surgical navigation based on preoperative patient images (e.g. SPECT/CT) is increasingly used to guide lesion localization in the operating room [50]. However, when we do not use GPS-navigation in combination with dynamic data, live updates such as road construction and traffic jams, can render the guidance

outdated. To this end, navigation extensions based on dynamic intraoperative fhSPECT and fhFluo imaging, provide a means to introduce the concept of “live updates” in the surgical navigation process. Just as a combination of satellite and local internet signals can drastically increase the precision of urban navigation due to their complementary natures [72], we reasoned the high resolution superficial nature of fluorescence can help refine the surgical navigation accuracy [33]–[36], a concept that is now extended with the fhFluo modality. Clinical studies are needed to determine if the proposed hybrid navigation setup should be pursued in a fully integrated fashion (i.e. fusion of fhSPECT and fhFluo visualizations) or in a sequential fashion where fhSPECT and fhFluo scans are acquired during different stages of the surgical procedure.

V. CONCLUSION

In this study, we introduced a novel method of fluorescence imaging (fhFluo), which can be applied during image-guided surgery. We demonstrated that the fhFluo approach (“pseudotomographic imaging”) could complement fhSPECT (“tomographic imaging”) during hybrid imaging and navigation studies. Having both fhSPECT and fhFluo available in a hybrid navigation setup: 1) combined the in-depth guidance of nuclear imaging with the high resolution of fluorescence imaging, 2) supported the differentiation between tissue attenuation of the different signals, 3) allowed multiplexing of different tracers, and 4) supported augmented and virtual reality multimodal visualization and guidance concepts.

ACKNOWLEDGMENT

The authors would like to gratefully acknowledge the surgical staff of the NKI-AVL (Amsterdam, the Netherlands) for assistance in the operating room. Furthermore, they would also like to thank Sven van Leeuwen (Interventional Molecular Imaging Laboratory, Department of Radiology, Leiden University Medical Center, Leiden, the Netherlands) and Michael Boonekamp (Department of Technical Services subsection Development, Leiden University Medical Center, Leiden, the Netherlands) for their assistance with the article illustrations and prototyping of the geometrical calibrators. Material support was provided by Eurorad (Eurorad S.A., Eckbolsheim, France) supporting the study with a prototype opto-nuclear probe, SurgicEye (SurgicEye GmbH, Munich, Germany) allowing the authors to run their own prototype software on the declipseSPECT and Hamamatsu (Hamamatsu Photonics kk., Hamamatsu, Japan) supporting the study with a prototype FIS-00 fluorescence camera system.

REFERENCES

- [1] T. Maurer *et al.*, “^{99m}Technetium-based prostate-specific membrane antigen–radioguided surgery in recurrent prostate cancer,” *Eur. Urol.*, vol. 75, no. 4, pp. 659–666, Apr. 2018.
- [2] E. S. Camillocci *et al.*, “A novel radioguided surgery technique exploiting β^- decays,” *Sci. Rep.*, vol. 4, Mar. 2014, Art. no. 4401.
- [3] S. Vidal-Sicart, M. Rioja, P. Paredes, M. Keshtgar, and R. Valdés Olmos, “Contribution of perioperative imaging to radioguided surgery,” *Quart. J. Nucl. Med. Mol. Imag.*, vol. 58, no. 2, pp. 140–160, Jun. 2014.

- [4] V. M. Moncayo, A. L. Alazraki, N. P. Alazraki, and J. N. Aarsvold, "Sentinel lymph node biopsy procedures," *Seminars Nucl. Med.*, vol. 47, no. 6, pp. 595–617, Nov. 2017.
- [5] R. A. V. Olmos, D. D. D. Riethbergen, and S. Vidal-Sicart, "SPECT/CT and sentinel node lymphoscintigraphy," *Clin. Transl. Imag.*, vol. 2, no. 6, pp. 491–504, Dec. 2014.
- [6] K. Herrmann, O. Nieweg, and S. P. Povoski, *Radioguided Surgery: Current Applications and Innovative Directions in Clinical Practice*. Cham, Switzerland: Springer, 2016.
- [7] C. Bluemel, P. Matthies, K. Herrmann, and S. P. Povoski, "3D scintigraphic imaging and navigation in radioguided surgery: Freehand SPECT technology and its clinical applications," *Expert Rev. Med. Devices*, vol. 13, no. 4, pp. 339–351, 2016.
- [8] T. Wendler *et al.*, "First demonstration of 3-D lymphatic mapping in breast cancer using freehand SPECT," *Eur. J. Nucl. Med. Mol. Imag.*, vol. 37, no. 8, pp. 1452–1461, Aug. 2010.
- [9] F. W. van Leeuwen, J. C. Hardwick, and A. R. van Erkel, "Luminescence-based imaging approaches in the field of interventional molecular imaging," *Radiology*, vol. 276, no. 1, pp. 12–29, Jul. 2015.
- [10] I. Stoffels, J. Dissemont, T. Pöppel, D. Schadendorf, and J. Klode, "Intraoperative fluorescence imaging for sentinel lymph node detection: Prospective clinical trial to compare the usefulness of indocyanine green vs technetium Tc 99m for identification of sentinel lymph nodes," *JAMA Surg.*, vol. 150, no. 7, pp. 617–623, Jul. 2015.
- [11] A. Christensen *et al.*, "Feasibility of real-time near-infrared fluorescence tracer imaging in sentinel node biopsy for oral cavity cancer patients," *Ann. Surgical Oncol.*, vol. 23, no. 2, pp. 565–572, Feb. 2016.
- [12] G. KleinJan *et al.*, "The best of both worlds: A hybrid approach for optimal pre- and intraoperative identification of sentinel lymph nodes," *Eur. J. Nucl. Med. Mol. Imag.*, vol. 45, no. 11, pp. 1915–1925, Oct. 2018.
- [13] A. Bennàssar, A. Vilata, S. Puig, and J. Malvehy, "Ex vivo fluorescence confocal microscopy for fast evaluation of tumour margins during Mohs surgery," *Brit. J. Dermatology*, vol. 170, no. 2, pp. 360–365, Feb. 2014.
- [14] G. Widhalm *et al.*, "5-Aminolevulinic acid induced fluorescence is a powerful intraoperative marker for precise histopathological grading of gliomas with non-significant contrast-enhancement," *PLoS ONE*, vol. 8, no. 10, Oct. 2013, Art. no. e76988.
- [15] A. Corlu *et al.*, "Three-dimensional in vivo fluorescence diffuse optical tomography of breast cancer in humans," *Opt. Express*, vol. 15, no. 11, pp. 6696–6716, May 2007.
- [16] F. W. van Leeuwen, R. Valdés-Olmos, T. Buckle, and S. Vidal-Sicart, "Hybrid surgical guidance based on the integration of radionuclear and optical technologies," *Brit. J. Radiol.*, vol. 89, Jun. 2016, Art. no. 20150797.
- [17] M. C. Hekman *et al.*, "Tumor-targeted dual-modality imaging to improve intraoperative visualization of clear cell renal cell carcinoma: A first in man study," *Theranostics*, vol. 8, no. 8, pp. 2161–2170, Mar. 2018.
- [18] M. Markuszewski, W. Polom, W. Cytawa, P. Czapiewski, P. Lass, and M. Matuszewski, "Comparison of real-time fluorescent indocyanine green and (99m)Tc-nanocolloid radiotracer navigation in sentinel lymph node biopsy of penile cancer," *Clin. Genitourinary Cancer*, vol. 13, no. 6, pp. 574–580, Dec. 2015.
- [19] P. Meershoek *et al.*, "Robot-assisted laparoscopic surgery using DROP-IN radioguidance: First-in-human translation," *Eur. J. Nucl. Med. Mol. Imag.*, vol. 46, no. 1, pp. 49–53, Jan. 2018.
- [20] B. E. Schaafsma *et al.*, "Near-infrared fluorescence sentinel lymph node biopsy in vulvar cancer: A randomised comparison of lymphatic tracers," *BJOG: An Int. J. Obstetrics Gynaecology*, vol. 120, no. 6, pp. 758–764, May 2013.
- [21] P. Paredes *et al.*, "Role of ICG-^{99m}Tc-nanocolloid for sentinel lymph node detection in cervical cancer, a pilot study," *Eur. J. Nucl. Med. Mol. Imag.*, vol. 44, no. 11, pp. 1853–1861, Oct. 2017.
- [22] B. E. Schaafsma *et al.*, "Clinical trial of combined radio- and fluorescence-guided sentinel lymph node biopsy in breast cancer," *Brit. J. Surg.*, vol. 100, no. 8, pp. 1037–1044, Jul. 2013.
- [23] I. Stoffels, J. Leyh, T. Pöppel, D. Schadendorf, and J. Klode, "Evaluation of a radioactive and fluorescent hybrid tracer for sentinel lymph node biopsy in head and neck malignancies: Prospective randomized clinical trial to compare ICG-^{99m}Tc-nanocolloid hybrid tracer versus ^{99m}Tc-nanocolloid," *Eur. J. Nucl. Med. Mol. Imag.*, vol. 42, no. 11, pp. 1631–1638, Oct. 2015.
- [24] S. L. Bugby, J. Lees, and A. Perkins, "Hybrid intraoperative imaging techniques in radioguided surgery: Present clinical applications and future outlook," *Clin. Transl. Imag.*, vol. 5, no. 4, pp. 323–341, Aug. 2017.
- [25] J. P. Gambini and T. P. Quinn, "Hybrid tracers and devices for intraoperative imaging: The future for radioguided surgery?" *Clin. Transl. Imag.*, vol. 4, no. 5, pp. 343–351, Oct. 2016.
- [26] M.-A. Poumellec *et al.*, "Détection du ganglion sentinel dans le cancer du sein par sonde opto-nucléaire après injection de vert indocyanine et de technétium 99m," *Gynécologie Obstétrique Fertilité*, vol. 44, no. 4, pp. 207–210, Apr. 2016.
- [27] N. S. van den Berg *et al.*, "First-in-human evaluation of a hybrid modality that allows combined radio- and (near-infrared) fluorescence tracing during surgery," *Eur. J. Nucl. Med. Mol. Imag.*, vol. 42, no. 11, pp. 1639–1647, Oct. 2015.
- [28] S. Vidal-Sicart *et al.*, "Clinical use of an opto-nuclear probe for hybrid sentinel node biopsy guidance: First results," *Int. J. Comput. Assist. Radiol. Surg.*, vol. 14, no. 2, pp. 409–416, Feb. 2018.
- [29] H. G. Kang, S. H. Song, Y. B. Han, H.-Y. Lee, K. M. Kim, and S. J. Hong, "Proof-of-concept of a multimodal laparoscope for simultaneous NIR/gamma/visible imaging using wavelength division multiplexing," *Opt. Express*, vol. 26, pp. 8325–8339, 2018.
- [30] J. E. Lees *et al.*, "A multimodality hybrid gamma-optical camera for intraoperative imaging," *Sensors*, vol. 17, no. 7, p. 554, 2017.
- [31] K. Popovic, *Intraoperative Multimodal Imaging System for Surgical Guidance*. Charlottesville, VA, USA: Univ. Virginia, 2013.
- [32] G. H. KleinJan *et al.*, "Hybrid surgical guidance: Does hardware integration of γ - and fluorescence imaging modalities make sense?" *J. Nucl. Med.*, vol. 58, no. 4, pp. 646–650, Apr. 2017.
- [33] O. R. Brouwer *et al.*, "Image navigation as a means to expand the boundaries of fluorescence-guided surgery," *Phys. Med. Biol.*, vol. 57, no. 10, pp. 3123–3126, May 2012.
- [34] G. H. KleinJan *et al.*, "Toward (Hybrid) navigation of a fluorescence camera in an open surgery setting," *J. Nucl. Med.*, vol. 57, no. 10, pp. 1650–1653, Oct. 2016.
- [35] M. N. van Oosterom *et al.*, "Navigation of a robot-integrated fluorescence laparoscope in preoperative SPECT/CT and intraoperative freehand SPECT imaging data: A phantom study," *Proc. SPIE*, vol. 21, no. 8, 2016, Art. no. 086008.
- [36] M. N. van Oosterom *et al.*, "Navigation of fluorescence cameras during soft tissue surgery—is it possible to use a single navigation setup for various open and laparoscopic urological surgery applications?" *J. Urol.*, vol. 199, no. 4, pp. 1061–1068, Apr. 2017.
- [37] P. Meershoek *et al.*, "Multispectral-fluorescence imaging as a tool to separate healthy from disease-related lymphatic anatomy during robot-assisted laparoscopy," *J. Nucl. Med.*, vol. 59, no. 11, pp. 1757–1760, Nov. 2018.
- [38] A. Hartl, D. I. Shakir, R. Kojchev, N. Navab, S. I. Ziegler, and T. Lasser, "Freehand SPECT reconstructions using look up tables," *Proc. SPIE*, vol. 8316, Feb. 2012, Art. no. 83162H.
- [39] A. Hartl, D. I. Shakir, T. Lasser, S. I. Ziegler, and N. Navab, "Detection models for freehand SPECT reconstruction," *Phys. Med. Biol.*, vol. 60, no. 3, pp. 1031–1046, Feb. 2015.
- [40] T. Wendler *et al.*, "Towards intra-operative 3D nuclear imaging: Reconstruction of 3D radioactive distributions using tracked gamma probes," in *Proc. Int. Conf. Med. Image Comput. Comput.-Assist. Intervent.*, 2007, pp. 909–917.
- [41] F. Monge, D. I. Shakir, F. Lejeune, X. Morandi, N. Navab, and P. Jannin, "Acquisition models in intraoperative positron surface imaging," *Int. J. Comput. Assist. Radiol. Surg.*, vol. 12, no. 4, pp. 691–703, Apr. 2017.
- [42] L. A. Shepp and Y. Vardi, "Maximum likelihood reconstruction for emission tomography," *IEEE Trans. Med. Imag.*, vol. 1, no. 2, pp. 113–122, Oct. 1982.
- [43] M. N. van Oosterom, D. A. den Houting, C. J. van de Velde, and F. W. van Leeuwen, "Navigating surgical fluorescence cameras using near-infrared optical tracking," *J. Biomed. Opt.*, vol. 23, May 2018, Art. no. 056003.
- [44] T. Engelen *et al.*, "The next evolution in radioguided surgery: Breast cancer related sentinel node localization using a freehandSPECT-mobile gamma camera combination," *Amer. J. Nucl. Med. Mol. Imag.*, vol. 5, no. 3, pp. 233–245, Feb. 2015.
- [45] G. H. KleinJan, B. Karakullukçu, W. M. C. Klop, T. Engelen, N. S. van den Berg, and F. W. van Leeuwen, "Introducing navigation during melanoma-related sentinel lymph node procedures in the head-and-neck region," *EJNMMI Res.*, vol. 7, no. 1, p. 65, Aug. 2017.

- [46] N. S. van den Berg *et al.*, “(Near-Infrared) fluorescence-guided surgery under ambient light conditions: A next step to embedment of the technology in clinical routine,” *Ann. Surgical Oncol.*, vol. 23, no. 8, pp. 2586–2595, Aug. 2016.
- [47] G. H. KleinJan *et al.*, “Fluorescence guided surgery and tracer-dose, fact or fiction?” *Eur. J. Nucl. Med. Mol. Imag.*, vol. 43, no. 10, pp. 1857–1867, Sep. 2016.
- [48] M. N. van Oosterom *et al.*, “U-SPECT-BioFluo: An integrated radionuclide, bioluminescence, and fluorescence imaging platform,” *EJNMMI Res.*, vol. 4, p. 56, Oct. 2014.
- [49] N. Van Den Berg *et al.*, “Hybrid tracers for sentinel node biopsy,” *Quart. J. Nucl. Med. Mol. Imag.*, vol. 58, no. 2, pp. 193–206, Jun. 2014.
- [50] M. N. van Oosterom, H. G. van der Poel, N. Navab, C. J. H. van de Velde, and F. W. B. van Leeuwen, “Computer-assisted surgery: Virtual- and augmented-reality displays for navigation during urological interventions,” *Current Opinion Urol.*, vol. 28, no. 2, pp. 205–213, Mar. 2018.
- [51] O. R. Brouwer *et al.*, “Feasibility of intraoperative navigation to the sentinel node in the groin using preoperatively acquired single photon emission computerized tomography data: Transferring functional imaging to the operating room,” *J. Urol.*, vol. 192, no. 6, pp. 1810–1816, Dec. 2014.
- [52] V. Cuplov, I. Buvat, F. Pain, and S. Jan, “Extension of the GATE Monte-Carlo simulation package to model bioluminescence and fluorescence imaging,” *Proc. SPIE*, vol. 19, no. 2, Feb. 2014, Art. no. 026004.
- [53] H. G. Kang, S. H. Song, Y. B. Han, K. M. Kim, and S. J. Hong, “Lens implementation on the GATE Monte Carlo toolkit for optical imaging simulation,” *J. Biomed. Opt.*, vol. 23, no. 2, Feb. 2018, Art. no. 026003.
- [54] C. G. Ethun and K. A. Delman, “The importance of surgical margins in melanoma,” *J. Surgical Oncol.*, vol. 113, no. 3, pp. 339–345, Mar. 2016.
- [55] S. B. Ravi and S. Annavajjula, “Surgical margins and its evaluation in oral cancer: A review,” *J. Clin. Diagnostic Res.*, vol. 8, no. 9, pp. ZE01–ZE05, Sep. 2014.
- [56] E. Sadot *et al.*, “Resection margin and survival in 2368 patients undergoing hepatic resection for metastatic colorectal cancer: Surgical technique or biologic surrogate?” *Ann. Surg.*, vol. 262, no. 3, pp. 476–485, Sep. 2015.
- [57] S. Yamada *et al.*, “Estimation of the width of free margin with a significant impact on local recurrence in surgical resection of oral squamous cell carcinoma,” *Int. J. Oral Maxillofacial Surg.*, vol. 45, no. 2, pp. 147–152, Feb. 2016.
- [58] T. Wendler, J. Traub, S. I. Ziegler, and N. Navab, “Navigated three dimensional beta probe for optimal cancer resection,” in *Medical Image Computing and Computer-Assisted Intervention*, vol. 9. Berlin, Germany: Springer, 2006, pp. 561–569.
- [59] K. Roessler, A. Becherer, M. Donat, M. Cejna, and I. Zachenhofer, “Intraoperative tissue fluorescence using 5-aminolevulinic acid (5-ALA) is more sensitive than contrast MRI or amino acid positron emission tomography ((¹⁸F)-FET PET) in glioblastoma surgery,” *Neurological Res.*, vol. 34, no. 3, pp. 314–317, Apr. 2012.
- [60] D. M. van Willigen *et al.*, “Multispectral fluorescence guided surgery; A feasibility study in a phantom using a clinical-grade laparoscopic camera system,” *Amer. J. Nucl. Med. Mol. Imag.*, vol. 7, no. 3, pp. 138–147, Jul. 2017.
- [61] A. K. Glaser *et al.*, “Light-sheet microscopy for slide-free non-destructive pathology of large clinical specimens,” *Nature Biomed. Eng.*, vol. 1, no. 7, p. 0084, Jul. 2017.
- [62] G. H. KleinJan *et al.*, “Optimisation of fluorescence guidance during robot-assisted laparoscopic sentinel node biopsy for prostate cancer,” *Eur. Urol.*, vol. 66, no. 6, pp. 991–998, Dec. 2014.
- [63] O. R. Brouwer *et al.*, “A hybrid radioactive and fluorescent tracer for sentinel node biopsy in penile carcinoma as a potential replacement for blue dye,” *Eur. Urol.*, vol. 65, no. 3, pp. 600–609, Mar. 2014.
- [64] A. Markus *et al.*, “Sentinel lymph node biopsy in endometrial and cervical cancers using freehand SPECT—first experiences,” *Gynecological Surg.*, vol. 13, no. 4, pp. 499–506, Nov. 2016.
- [65] J. Müller *et al.*, “Handheld single photon emission computed tomography (handheld SPECT) navigated video-assisted thoracoscopic surgery of computer tomography-guided radioactively marked pulmonary lesions,” *Interact. Cardiovascular Thoracic Surg.*, vol. 23, no. 3, pp. 345–350, May 2016.
- [66] N. C. Hall *et al.*, “Intraoperative use of a portable large field of view gamma camera and handheld gamma detection probe for radioguided localization and prediction of complete surgical resection of gastrinoma: Proof of concept,” *J. Amer. College Surgeons*, vol. 221, no. 2, pp. 300–308, Aug. 2015.
- [67] A. Azhdarinia, P. Ghosh, S. Ghosh, N. Wilganowski, and E. M. Sevick-Muraca, “Dual-labeling strategies for nuclear and fluorescence molecular imaging: A review and analysis,” *Mol. Imag. Biol.*, vol. 14, no. 3, pp. 261–276, Jun. 2012.
- [68] J. Kuil, A. H. Velders, and F. W. van Leeuwen, “Multimodal tumor-targeting peptides functionalized with both a radio- and a fluorescent label,” *Bioconjug. Chem.*, vol. 21, no. 10, pp. 1709–1719, Oct. 2010.
- [69] M. Schottelius *et al.*, “Synthesis and preclinical characterization of the PSMA-targeted hybrid tracer PSMA-I&F for nuclear and fluorescence imaging of prostate cancer,” *J. Nucl. Med.*, vol. 60, no. 1, pp. 71–78, Jan. 2019.
- [70] C. Santini *et al.*, “Evaluation of a fluorescent and radiolabeled hybrid somatostatin analog *in vitro* and in mice bearing H69 neuroendocrine xenografts,” *J. Nucl. Med.*, vol. 57, no. 8, pp. 1289–1295, Aug. 2016.
- [71] X. Wang, M. B. Aldrich, M. V. Marshall, and E. M. Sevick-Muraca, “Preclinical characterization and validation of a dual-labeled trastuzumab-based imaging agent for diagnosing breast cancer,” *Chin. J. cancer Res.*, vol. 27, no. 1, pp. 74–82, Feb. 2015.
- [72] K. Nur, S. Feng, C. Ling, and W. Ochieng, “Integration of GPS with a WiFi high accuracy ranging functionality,” *Geo-Spatial Inf. Sci.*, vol. 16, no. 3, pp. 155–168, 2013.